ELSEVIER

Journal of Alloys and Compounds 434–435 (2007) 244–247

Journal of ALLOYS AND COMPOUNDS

www.elsevier.com/locate/jallcom

Crystallization steps in Zr- and Hf-based bulk metallic glasses

L.C. Damonte *, L. Mendoza-Zélis

Physics Department, U.N.L.P. and IFLP, CONICET, 1900 La Plata, Argentina

Available online 10 October 2006

Abstract

Different Zr- and Hf-based amorphous alloys were prepared by melt-spinning, mechanical milling and copper mold casting to compare their devitrification behaviour. The perturbed angular correlation technique was applied to characterize the local order in these amorphous samples and its evolution with temperature. The crystallisation process, being a complex mechanism in these multicomponent alloys, is analyzed in detail. At intermediate stages metastable phases and nuclei of intermetallic compounds are found. The hyperfine parameters of the final products are compared with those of well defined crystalline alloys.
© 2006 Elsevier B.V. All rights reserved.

Keywords: Short range order; Crystallization; Amorphous alloys; Perturbed angular correlations; Bulk metallic glasses

1. Introduction

Crystallization behaviour of bulk metallic glasses shows a variety of characteristic features: phase separation, incipient nucleation, formation of metastable phases, etc. The occurrence of a given evolution depends on composition, heat treatment, oxygen content and, frequently, the addition of other elements. It is also known that in Zr–Al–Cu–Ni bulk glasses small amounts of oxygen reduce the thermal stability and promote the formation of quasicrystalline or metastable Ti_2Ni-type phases. In a similar way, the preparation method may influence the crystallisation process. Recently, it was argued that the possibility of phase decomposition in the supercooled liquid state may influence the crystallization process [1,2]. These facts renew the interest in the relationship between short-range order in metallic glasses and the formation of metastable aperiodically ordered phases.

Perturbed angular correlations as one of the electric field gradient-sensitive techniques, have already been applied to the analysis of the local atomic order in various bulk metallic glasses alloys [3–6]. In this work we applied this technique to analyze the short-range order in different Zr- and Hf-based multicomponent amorphous alloys in the supercooled liquid state and after different heat treatments.

2. Experimental

Samples were prepared by different methods from purified elemental metals. The studied systems were: copper-mold cast rod of $Zr_{53}Hf_2Cu_{30}Al_{10}Ni_5$ (Z55) [4]; mechanically alloyed powders of $Zr_{63}Hf_2Cu_{17.5}Al_{7.5}Ni_{10}$ (Z65) and $Hf_{65}Al_{7.5}Cu_{17.5}Ni_{10}$ (H65) [5] and melt spun ribbons of $Hf_{55}Cu_{30}Al_{10}Ni_5$ (H55), $Zr_{52.5}Hf_2Ti_{7.5}Cu_{20}Al_{10}Ni_8$ (ZTI) [6]. The 2 at.% addition of hafnium in Zr-based alloys is necessary for the PAC measurements. Details on the equipment setup and data analysis can be found in previous works [2,5]. The quadrupolar frequency, ω_Q, resulting from the PAC spectra after a least-squares fitting procedure, gives information on the electric field gradient (EFG) generated by the surroundings of the probe atom by means of $\omega_Q = eQV_{zz}/40\hbar$ (Q is the nuclear quadrupole moment). Other obtained parameter is the predicted relative width $\delta = \Delta_{zz}/V_{zz}$, which indicates how defined is the involved structural site, and the asymmetry parameter, defined by $\eta = (V_{xx} - V_{yy})/V_{zz}$.

The samples were annealed at temperatures 40–60 K below the first exothermic peak at increasing periods of time. Also heat treatments during 1 h at increasing temperatures were done in order to obtain the full crystallization of the samples.

3. Results and discussion

The short-range order thermal evolution at temperatures below the first exothermic peak in both Zr- and Hf-based alloys were analysed. Fig. 1 shows the resulting Fourier transform of the PAC spectra obtained for all composition at a selected step of crystallization. In Table 1, the details on the specific heat treatments is display together with their corresponding crystallization temperatures (defined by the onset of the exothermic events). The common feature in all the alloys annealed below the first exothermic temperature peak is the presence of wide

* Corresponding author.
E-mail addresses: damonte@fisica.unlp.edu.ar (L.C. Damonte), mendoza@fisica.unlp.edu.ar (L. Mendoza-Zélis).

0925-8388/$ – see front matter © 2006 Elsevier B.V. All rights reserved.
doi:10.1016/j.jallcom.2006.08.119

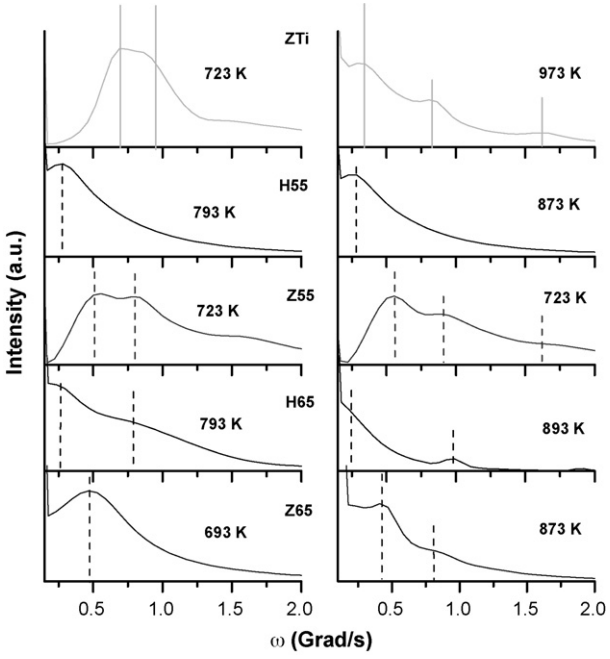

Fig. 1. Fourier transform of PAC spectra for annealed amorphous alloys. Left, below the first crystallization temperatures (see Table 1). Right, after prolonged heat treatments at the indicated temperatures. The vertical lines indicate the central values of the frequency distributions.

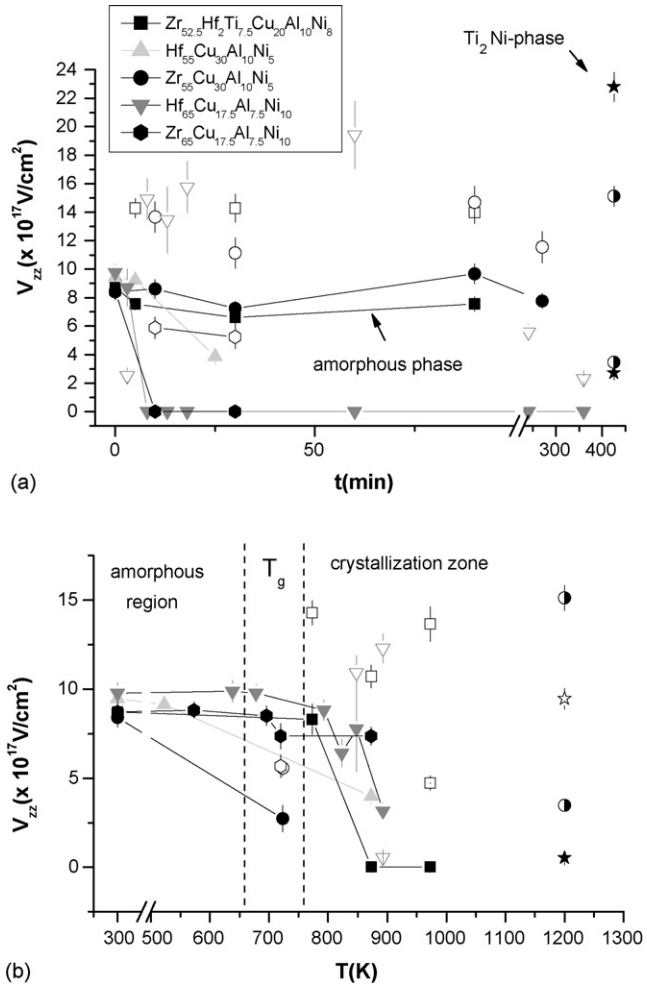

Fig. 2. The central EFG distribution value evolution for all the analyzed amorphous alloys with: (a) increasing time and (b) increasing temperature. Full symbols, the majority EFG component (right lines are to guide the eyes); open symbols, phases at minority population fraction. Also shown are: tetragonal $Hf_2(Zr_2)Cu$ (full start in (b)), $Hf_2(Zr_2)Ni$ (open start in (b)), $Hf_6(Zr_6)NiAl_2$ (semi full circles) and a metastable Ti_2Ni-type phase (full starts in (a)).

distributions of frequencies (left side in Fig. 1). It is observed that the H55 and Z65 alloys display one site distribution meanwhile a two site distribution is clearly evident in the other three. As increasing annealing time the central values of these distributions changes to values corresponding to more defined structural sites similar to those in intermetallic compounds, reducing also their relative width. Similar changes are observed for isochronal annealing at increasing different temperatures. On the right side of Fig. 1 the resulting Fourier transforms of the PAC spectra corresponding to the last annealing step done on the different samples is shown. From the figure the more defined probe atom environments is evident.

Fig. 2 shows the evolution with time (Fig. 2a) and with temperature (Fig. 2b) of the central EFG distribution value for all the analyzed amorphous alloys obtained after least-square fittings of the PAC spectra. Full symbols represent the majority EFG component; open symbols are the corresponding ones for phases at minority population fraction. According to the results obtained from PAC spectra analysis, three zones can be distinguished in Fig. 2b. The amorphous region, where the spectra are characterized by a wide distribution of quadrupolar frequencies, well described by a distribution function $P(V_{zz}, \eta)$ based on a dense random packing (DRP) of ions [3–6]. An intermediate region, corresponding to the glass transition temperatures of the different amorphous alloys. When samples are annealed at these temperatures the results are one or two wide distributions of frequencies, but they cannot be always described by a DRP model [5,6]. We have named crystallization zone that

Table 1
Details of heat treatments done on the studied amorphous alloys

Sample	Annealed treatment	T_{x1} (K)	T_{x2} (K)	Intermediate phases	Final phases
$Zr_{52.5}Hf_2Ti_{7.5}Cu_{20}Al_{10}Ni_8$	5 min × 723 K	716	759	Ti_2Ni-phase + amorphous	t-$Zr_2Cu + Zr_6NiAl_2$
$Hf_{55}Cu_{30}Al_{10}Ni_5$	25 min × 793 K	855	–	Nuclei Hf_6NiAl_2	Hf_6NiAl_2
$Zr_{53}Hf_2Cu_{30}Al_{10}Ni_5$	30 min × 723 K	767	–	Ti_2Ni-phase or nuclei Zr_6NiAl_2	Zr_6NiAl_2
$Hf_{65}Al_{7.5}Cu_{17.5}Ni_{10}$	8 min × 793 K	823	873	t-$Hf_2Cu + Ti_2Ni$-phase (minor)	t-$Hf_2Cu + Hf_6NiAl_2$
$Zr_{63}Hf_2Cu_{17.5}Al_{7.5}Ni_{10}$	10 min × 693 K	728	773	t-Zr_2Cu + nuclei Zr_6NiAl_2	t-$Zr_2Cu + Zr_6NiAl_2$

T_{x1} and T_{x2} are the first and second crystallization temperatures (defined by the onset of the exothermic events). Also the observed intermediate and final phases are shown.

temperature region were the PAC spectra are well described by Gaussian distributions of frequencies more similar to the ones corresponding to the final crystallization products.

Also shown in Fig. 2 are the quadrupole parameters corresponding to stable intermetallic compounds already characterized by PAC. The tetragonal $Hf_2(Zr_2)Cu$ (full start in Fig. 2b) and $Hf_2(Zr_2)Ni$ (open start in Fig. 2b) characterized by a unique EFG [7,8]; $Hf_6(Zr_6)NiAl_2$ (semi full circles in Fig. 2) which have two inequivalent structural sites [9] and a metastable Ti_2Ni-phase (full starts in Fig. 2a) whose quadrupole parameters are obtained from an isomorphous compound Hf_2Fe [6].

Although at a first sight a great dispersion of values is evident from Fig. 2, some trends can be inferred. For H55 sample (upper triangle) at first stage of crystallization one frequency distribution has observed, being its mean value close to the low EFG component of the Hf_6NiAl_2 intermetallic compound ($V_{zz} = 4 \times 10^{17}$ V/cm^2). With further annealings no changes are produced only a slightly diminution in its wide width.

In the case of Z65 (hexagon), although the Fourier transform displays one site wide distribution, the fit yield two EFG component with low central values. One distribution centered at zero frequency which is associated with nuclei of crystalline Zr_2Cu, characterized by a low EFG [7], in agreement with other reported results at first stage of crystallization in Zr–Al–Ni–Cu alloys [10,11]. The second EFG component (above 4×10^{17} V/cm^2) can be assigned to the structural site of low EFG component in Zr_6NiAl_2. X-ray diffractograms (not shown in this work) confirm the observed phases at this stage.

For ZTI, H65 and Z55 samples the intermediate stages are rather complicated, but they have a distinctive behaviour since all display a two widely distributed electrical field gradients. In the case of ZTI one of these distributions is characteristic of an amorphous phase [6]. For H65, one EFG distribution has a very low value, close to zero, which is assigned to tetragonal Hf_2Cu [7] similar to the one observed for Z65, since both compounds are isomorphous. The Z55 sample displays an EFG distribution which has a central value similar to the one of ZTI but not described by a DRP model. This component evolves, with further annealing, to the low EFG in Zr_6NiAl_2 ($V_{zz} = 4 \times 10^{17}$ V/cm^2). The assignment of the other resulting component (V_{zz} between 11×10^{17} and 19×10^{17} V/cm^2) in the three precedent alloys is rather ambiguous since the local environments for the metastable Ti_2Ni-type phase (22.8×10^{17} V/cm^2) and preclude nuclei of $Hf_6(Zr_6)NiAl_2$ (15×10^{17} V/cm^2) show some similarity. We analyzed the XRD patterns for ZTI and H65 samples at this annealing step and the corresponding diffraction peaks of the metastable phase are clearly visible (Fig. 3) together with some broad other crystalline peaks such as $Hf_2(Zr_2)Cu$ and $Hf_6(Zr_6)NiAl_2$; in ZTI the characteristic amorphous halo is also seen [6]. However, as prolonged higher temperature treatments the Ti_2Ni-phase evolved to crystalline $Hf_6(Zr_6)NiAl_2$ since both hyperfine parameters, EFG and asymmetry parameter (η) are well defined, allowing us to make a choice from the different phase options.

Metastable Zr_2Ni (Ti_2Ni-type phase) and tetragonal Zr_2Cu have been previously reported as intermediate and final crystallization products in Zr-based alloys with similar composition as

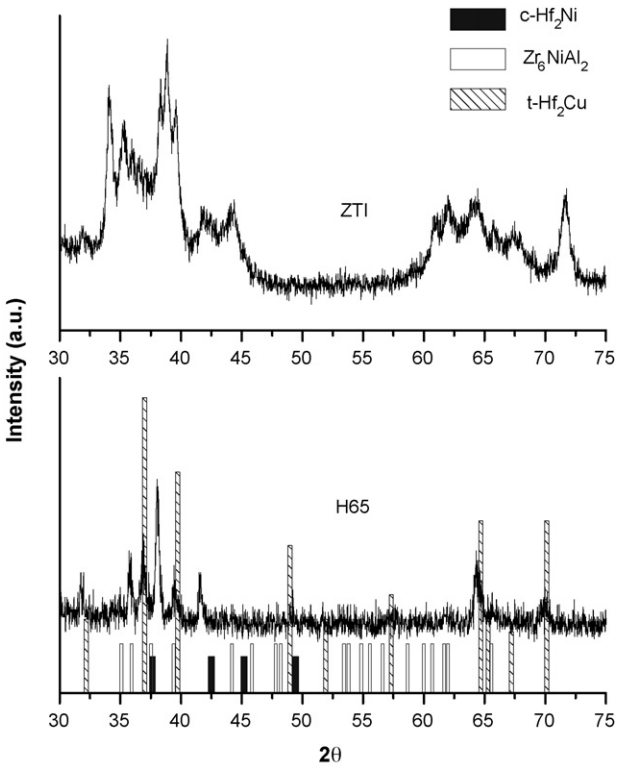

Fig. 3. XRD diffraction patterns for: above, $Zr_{52.5}Hf_2Ti_{7.5}Cu_{20}Al_{10}Ni_8$ (ZTI) and bottom $Hf_{65}Al_{7.5}Cu_{17.5}Ni_{10}$ (H65).

in sample Z55 [12,13]. In the case of the alloys containing Ti, several authors have suggested the presence of metastable phases upon crystallization [14–16]. Table 1 also shows the intermediate and final phases as identified by PAC and XRD patterns according to the above discussion.

In summary, we have observed that the metastable Ti_2Ni-phase formed during intermediate devitrification steps in melt spun ZTI, mechanical milled H65 and copper mold Z55 alloys. This result contrast with what happened in others Zr-based alloys [1] where quasicrystalline phase formation is observed as first stages of crystallization only in amorphous synthesized directly from the liquid state. Phase separation prior to the crystallization steps was only observed in ZTI sample where an amorphous phase coexists with the metastable Ti_2Ni-phase as was observed by other authors [2]. The EFG in this metastable phase has different value from the EFG existing in the amorphous phase, indicating no linkage to the short-range order in the glassy state. Similarly, Mattern et al. [16] in $Zr_{60}Ti_2Cu_{20}Ni_8Al_{10}$, a close composition to ZTI sample, have observed by X-ray synchrotron diffraction no structural change between glassy and supercooled liquid states.

4. Conclusion

Analysis on the short-range order in several amorphous alloys by means of the PAC hyperfine technique allows us to conclude:

- Thermal annealings below the first crystallization temperature leads to the precipitation of Ti_2Ni-type metastable phase and

nuclei of the intermetallic compounds as expected from the equilibrium phase diagram.
- The short-range order in the metastable phase seems to have no correlation with the existing one in the amorphous or supercooled liquid state.

Acknowledgments

We are grateful to the IFW (Dresden, Germany) staff, especially to J. Eckert, for the preparation and thermal characterization of samples. This work was supported by Consejo Nacional de Investigaciones Científicas y Técnicas (CONICET) under grant PIP 2000 no. 02946, and Agencia Nacional de Promoción Científica y Técnica (ANPCYT) under grant no. 03-12816, Argentine.

References

[1] D.J. Sordelet, E. Rozhkova, M.F. Besser, M.J. Kramer, J. Non-Cryst. Solids 334–335 (2004) 263.
[2] K. Kajiwara, M. Ohnuma, T. Ohkubo, D.H. Ping, K. Hono, Mater. Sci. Eng. A 375–377 (2004) 738.
[3] L.C. Damonte, L.A. Mendoza-Zélis, J. Non-Cryst. Solids 351 (2005) 668–672.
[4] L.C. Damonte, L.A. Mendoza-Zélis, S. Deledda, J. Eckert, Mater. Sci. Eng. A 343 (2003) 194–198.
[5] L.C. Damonte, L.A. Mendoza-Zélis, J. Eckert, Mater. Sci. Eng. A 278 (2000) 16.
[6] L.C. Damonte, M.A. Bab, L.A. Mendoza-Zélis, S. Deledda, J. Eckert, J. Met. Nanocryst. Mater. 20–21 (2004) 499–504.
[7] L.C. Damonte, L. Mendoza-Zélis, A.R. López García, Phys. Rev. B 39 (1989) 12492.
[8] L.C. Damonte, L.A. Mendoza-Zélis, A.R. López García, E.D. Cabanillas, Phys. Rev. B 46 (1992) 13767.
[9] L.C. Damonte, L.A. Mendoza-Zélis, Hyp. Int. 158 (2004) 317–322.
[10] U. Köster, J. Meinhardt, S. Roos, A. Rüdiger, Mater. Sci. Forum 225–227 (1996) 311.
[11] H. Schumacher, U. Herr, D. Oelgeschlaeger, A. Traverse, K. Samwer, J. Appl. Phys. 82 (1997) 155.
[12] A.R. Yavari, A. Le Moulec, A. Inoue, J. Saida, C. Li, J. Walter, F. Botta, G. Vaughan, A. Kvick, Mater. Sci. Forum 343–346 (2000) 151.
[13] N. Ismail, M. Uhlemann, A. Gebert, J. Eckert, J. Alloys Compd. 298 (2000) 146.
[14] A.R. Yavari, A. Le Moulec, A. Inoue, J. Walter, F. Botta, G. Vaughan, A. Kvick, Mater. Sci. Eng. A 304–306 (2001) 34–38.
[15] L.Q. Xing, J. Eckert, W. Löser, Ann. Chim. Sci. Mater. 27 (2002) 69–75.
[16] N. Mattern, J. Sakowski, U. Kühn, H. Vinzelberg, J. Eckert, J. Non-Cryst. Solids 345–346 (2004) 758–761.